SF2A 2017
C. Reylé, P. Di Matteo, F. Herpin, É. Lagadec, A. Lançon, Z. Meliani, F. Royer (eds)

HIGH-CONTRAST IMAGING WITH THE JWST-NIRSPEC INTEGRAL FIELD UNIT

M. Ygouf[1], C. Beichman,[1], K. Hodapp[2] and T. Roellig[3]

Abstract. With its integral field unit, the near-infrared spectrograph NIRSPEC on JWST will allow to measure high-resolution spectra into the $3-5\,\mu$m range with an increased sensitivity over ground-based systems. This capability will considerably extend our knowledge of brown dwarfs and bright exoplanets at large separations from their host star. But because there is not any coronagraph on NIRSPEC , the performance in term of contrast at close separation will be extremely limited. In this communication, we explore possibilities to further push this limitation by exploiting the wavelength diversity offered by the spectral differential imaging strategy.

Keywords: JWST , NIRSPEC , IFU , Exoplanets, Brown Dwarfs, Direct Imaging, Post-Processing, Spectral Differential Imaging

1 Introduction

The integral field units (IFU s) on board of JWST (Gardner et al. 2009) offer a chance to measure high-resolution spectra of brown dwarfs and bright exoplanets in the near-IR for NIRSPEC (Ferruit et al. 2012) and in the mid-IR for MIRI (Wright et al. 2008). To achieve this, there is a need for techniques of post-processing to subtract the starlight while preserving the flux from the companion. This can be done by implementing observing strategies that introduce diversity in the data.

The spectral differential imaging (SDI) strategy exploit the wavelength diversity offered by an IFU . Empirical methods of post-processing have been used to subtract the starlight from coronagraphic or non-coronagraphic images in the focal plane (Sparks & Ford 2002; Lafrenière et al. 2007; Soummer et al. 2012). These methods are entirely based on starlight calibration in the focal plane, which cause part or totality of the planet signal to be subtracted in the process. To avoid this, there have been some attempts to model the off-axis PSF , using forward modelling (Soummer et al. 2012; Pueyo et al. 2014). Although this approach is useful for characterization (Pueyo et al. 2014; Ygouf et al. 2015), it can only work with SDI if there is a high correlation between the pattern of starlight residuals at different wavelengths. Even though the residual instrumental aberrations are responsible for these starlight residuals, none of these post-processing methods use a model of imaging that takes these aberrations as parameters. As a consequence, prior information inferred from our knowledge of the instrument can not be used as an input for post-processing.

An optimal post-processing technique would handle these limitations of the current techniques of post-processing. Ygouf et al. (2013) have developed the technique called MEDUSAE (*Multispectral Exoplanet Detection Using Simultaneous Aberration Estimation*) in a Bayesian framework, based on an analytical model of multispectral coronagraphic imaging and an inversion algorithm, to estimate jointly the instrumental aberrations and the circumstellar scene in order to separate these two contributions (Ygouf et al. 2013; Ygouf 2013). The inversion algorithm is based on a maximum-a-posteriori estimator, which measures the discrepancy between the multispectral data from an IFU and the imaging model. It is then possible to retrieve, from multispectral images, an estimation of the aberration map and of the position and flux of the companions at each wavelength and thus their spectra.

For the first time, we applied the MEDUSAE technique on non-coronagraphic JWST NIRSPEC IFU images. In the following sections, we describe two NIRCAM GTO programs that will make use of the NIRSPEC IFU

[1] IPAC, Caltech, 1200 E. California Blvd., Pasadena, CA 91125, USA
[2] Institute for Astronomy, University of Hawaii, 640 N. Aohoku Place, Hilo, HI 96720, USA
[3] NASA Ames Research Center, MS 245-6, Moffett Field, CA 94035-1000, USA

to further characterize known exoplanets and brown dwarfs with the NIRSPEC IFU ; we present the MEDUSAE technique before describing our simulated data; finally, we implement the technique on these simulated data to estimate jointly the instrumental aberrations and some injected point sources.

2 Direct Imaging of Exoplanet and Brown Dwarfs in the NIRCam GTO Program

The NIRCAM GTO team (PI : Marcia Rieke) designed two programs to image directly exoplanet and brown dwarfs with the NIRSPEC IFU :

- The *Spectroscopy of Young, Widely Separated Planets* led by Klaus Hodapp. The goal of this program is to understand the spectra of self-luminous, fairly young objects below the deuterium burning limit throughout their contraction and cooling.
- The *Y Dwarf Observations with* JWST led by Tom Roellig. The goal of this program is to understand the nature of the coolest brown dwarfs - their formation, their atmospheres, including their composition, temperature, pressure structures, and the nature of any clouds that may be present.

The methodology for these two programs is to obtain NIRSPEC IFU R=2700 spectra to allow direct imaging and spectroscopy. The use of NIRSPEC will thus extend the measurements into the $3-5\,\mu$m range with a substantial sensitivity advantage over competing ground-based systems. In the following, we apply for the first time the MEDUSAE technique on non-coronagraphic images for the preparation of GTO -NIRCAM observations with NIRSPEC .

3 The MEDUSAE technique

MEDUSAE was developed in the context of a coronagraphic instrument and is thus based on an analytical model of multispectral coronagraphic imaging (Ygouf et al. 2013). Here, in the context of the NIRSPEC IFU , we slightly change the model to deal with non-coronagraphic images. We assume that, for an image at the wavelength λ, the direct model is the following sum of three terms, separating the contributions of the star, the circumstellar source and noise n_λ:

$$i_\lambda(\alpha) = f^*_\lambda \cdot h^{nc}_\lambda(\alpha) + [o_\lambda \star h^{nc}_\lambda](\alpha) + n_\lambda(\alpha), \tag{3.1}$$

where $i_\lambda(\alpha)$ is the data, f^*_λ is the star flux at wavelength lambda and $h^{nc}_\lambda(\alpha)$, the non-coronagraphic point spread function (PSF). The expression of the non-coronagraphic PSF is $h^{nc}_\lambda = A_n A^*_n$, with $A_n(\alpha) = \mathrm{TF}^{-1}\left[\mathcal{P}(\rho)\, e^{j\phi(\rho)}\right]$, $\mathcal{P}(\rho)$ the telescope pupil and the OPD map $\phi(\rho) = 2\pi\frac{\delta(\rho)}{\lambda}$. $\mathrm{TF}[.]$ denotes the Fourier Transform.

Following the Bayesian inverse problem approach, solving the inverse problem consists in finding the unknowns, firstly the object characteristics $o(\alpha,\lambda) = \{o_\lambda(\alpha)\}_\lambda$, secondly the parameters the PSF $h^{nc}_\lambda(\delta)$ (namely the OPD map) and $f^*(\lambda) = \{f^*_\lambda\}_\lambda$, which are the most likely given the data and our prior information about the unknowns. This boils down to minimizing the following criterion:

$$J(o, f^*, \delta) = \sum_\lambda \sum_\alpha \frac{1}{2\sigma^2_{n,\lambda}(\alpha)} |i_\lambda - f^*_\lambda \cdot h^{nc}_\lambda(\delta) - o_\lambda \star h^{nc}_\lambda(\delta)|^2(\alpha) + R_o + R_{f^*} + R_\delta + \cdots. \tag{3.2}$$

This criterion is the sum of two terms: the data fidelity term, which measures the distance between the data and the imaging model, and a non-exhaustive list of regularization terms on our unknowns R_o, R_{f^*}, R_δ. The structure of the joint criterion of Eq. (3.2) prompted us to adopt an estimation of wavefront and object that alternates between estimation of the aberrations, assuming that the object is known (multispectral *phase retrieval*) and estimation of the object assuming that the aberrations are known (*multispectral deconvolution*). To minimize the criterion, we used the Variable Metric with Limited Memory and Bounds (VMLM-B) (Thiébaut 2002). More information about the regularization terms, constraints and minimization scheme can be found in Ygouf et al. (2013).

4 Simulations

Using the image formation model of equation (3.1), we simulate a data cube of 30 images typical of the NIRSPEC instrument. We choose pixel indicator functions as the basis for the phase rather than, e.g., a truncated basis

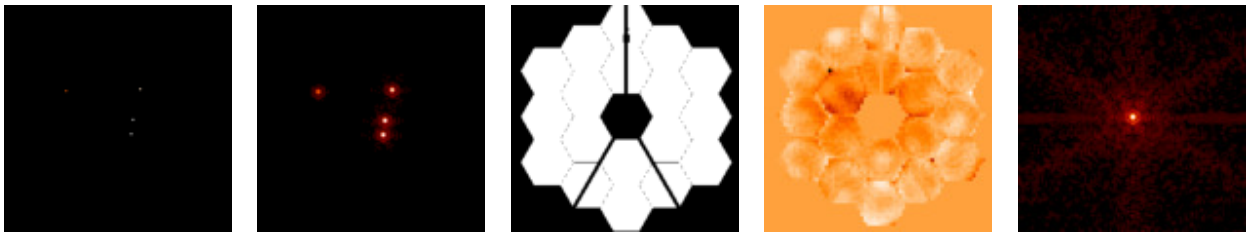

(a) Object map with four planets (b) Image of the object map in the focal plane (c) JWST pupil (d) Aberration map (e) Image of the NIRSPEC PSF

Fig. 1. Simulations of NIRSpec-like images at $\lambda = 3\,\mu$m. (a) Simulated object map and (b) associated image in the focal plane – the image in the focal plane is obtained by convolving the object map o_λ by the non-coronagraphic PSF h_λ^{nc} – (c) JWST pupil, (d) simulated aberrations and (e) associated PSF in the image focal plane.

of Zernike polynomials, in order to model and reconstruct phases with a high spatial frequency content. The hypothesis are typical of a NIRSPEC -like instrument: JWST pupil file (pupil_RevV.fits publicly available from the WEBBPSF package (Perrin et al. 2014)), OPD δ simulated with standard deviation of 125 nm (OPD file OPD_RevV_nirspec_125.fits publicly available from the WEBBPSF package (Perrin et al. 2014)), and a spectral range spanning from 3 to 5 µm. Photon noise is added to the data. We use 128×128 pixels to simulate our images, with an oversampling of 2 (0.05215 arcsec/pixel to be compared to 0.1 arcsec/pixel of the NIRSPEC detector). The number of unknowns to estimate for the aberration map is about 3×10^3. If we add the unknowns to estimate for the object map, which is 16×10^3, the total number of unknowns is about 2×10^4. Figure (1) shows the simulated object map (1(a)) and the associated image in the focal plane (1(b)). Figure 1(d) shows the simulated aberration map and the associated image of the speckle field in the focal plane (1(e)). Figure 2 shows the evolution of the NIRSPEC PSF with the wavelength. For an easier visualization, we represent the images in the focal plane and not the object map in the following.

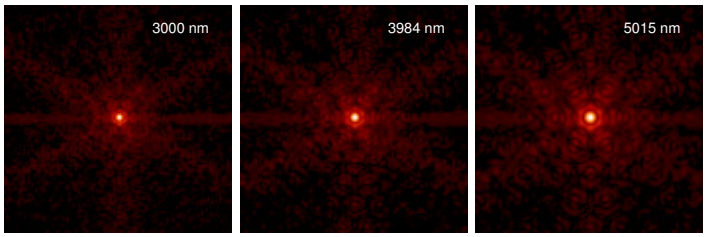

Fig. 2. Evolution of the NIRSpec-like PSF with the wavelength. Simulated images at 3, 4 and 5 µm. The two point sources that are closer to the star are completely buried in stellar halo. The two other point sources are barely visible. The dynamic range is adapted to the visualization.

5 Post-processing: preliminary results

From the simulated data cube we jointly estimate the OPD and the object maps using the MEDUSAE algorithm that we modified to deal with non-coronagraphic images. The results can be seen on Figure 3. For both the object and the OPD maps we compare the estimated map to the simulated one. The star halo is almost completely subtracted. Some starlight residuals can be observed. The four point sources are recovered but there is a non-negligible error on the object estimation. This error is all the more important as the point source is close to the star, which is a completely normal behavior of the algorithm. The global structure of the OPD is relatively well estimated. The residuals mostly comes from the error in planet flux estimation (sinusoidal structure). However, a few structures are not perfectly recovered. In Fig. 4 we plotted the contrast after post-processing with MEDUSAE . Contrast gain is comprised between 20 and 300 for separations spanning from 0.5 to 3".

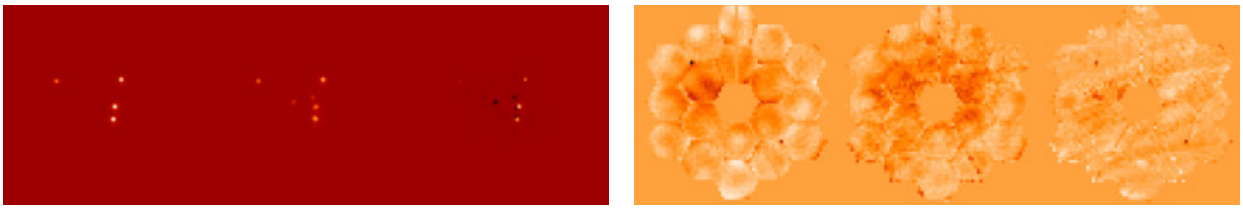

(a) Object estimation (b) OPD estimation

Fig. 3. Estimation of object and OPD maps (a) [Left] Simulated image in the focal plane of the object map, [center] estimated image and [right] difference between the simulated and estimated images at $\lambda = 3\,\mu$m. (b) [Left] Simulated OPD map, [center] estimated OPD map and [right] difference between the simulated and estimated images. The dynamic range is adapted to the visualization.

6 Conclusions and perspectives

We applied for the first time the MEDUSAE technique on non-coronagraphic images for the preparation of GTO - NIRCAM observations with NIRSPEC . The preliminary results are promising, demonstrating contrast gains up to 300 after post-processing as well as the ability to reconstruct the instrumental aberration map. The aberration map reconstruction shows the potential of the MEDUSAE technique for wavefront sensing and control of JWST . In future tests, we will consider simulation hypothesis that closer reflect the observing strategy we plan to implement in our NIRCAM -GTO programs and we will compare the performance of MEDUSAE to other observing strategies and corresponding post-processing techniques.

This research has made use of the WEBBPSF python package (Perrin et al. 2014). Most of the figures in this work were created using Matplotlib, a Python graphics environment (Hunter 2007).

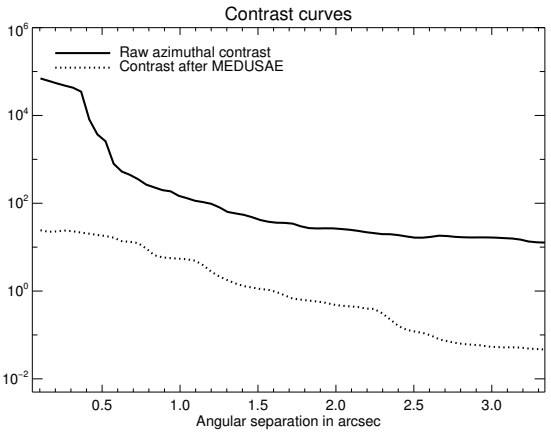

Fig. 4. Contrast curves before and after post-processing. Contrast curves are plotted by measuring the azimuthal 1-σ level of residual starlight.

References

Ferruit, P., Bagnasco, G., Barho, R., et al. 2012, in SPIE Astronomical Telescopes+ Instrumentation, International Society for Optics and Photonics, 84422O–84422O

Gardner, J. P., Mather, J. C., Clampin, M., et al. 2009, Astrophysics in the Next Decade, 1

Hunter, J. D. 2007, Computing In Science & Engineering, 9, 90

Lafrenière, D., Marois, C., Doyon, R., Nadeau, D., & Artigau, É. 2007, Astrophys. J., 660, 770

Perrin, M. D., Sivaramakrishnan, A., Lajoie, C.-P., et al. 2014, in Space Telescopes and Instrumentation 2014: Optical, Infrared, and Millimeter Wave, Vol. 9143, International Society for Optics and Photonics, 91433X

Pueyo, L., Soummer, R., Hoffmann, J., et al. 2014, ArXiv e-prints

Soummer, R., Pueyo, L., & Larkin, J. 2012, Astrophys. J. Lett., 755, L28

Sparks, W. B. & Ford, H. C. 2002, Astrophys. J., 578, 543

Thiébaut, E. 2002, in Society of Photo-Optical Instrumentation Engineers (SPIE) Conference Series, Vol. 4847, Society of Photo-Optical Instrumentation Engineers (SPIE) Conference Series, ed. J.-L. Starck & F. D. Murtagh, 174–183

Wright, G., Reike, G., Barella, P., et al. 2008, in Space Telescopes and Instrumentation 2008: Optical, Infrared, and Millimeter, Vol. 7010, International Society for Optics and Photonics, 70100T

Ygouf, M. 2013, PhD thesis, Université de Grenoble

Ygouf, M., Mugnier, L. M., Mouillet, D., Fusco, T., & Beuzit, J.-L. 2013, Astronomy & Astrophysics, 551, A138

Ygouf, M., Mugnier, L. M., Mouillet, D., Fusco, T., & Beuzit, J.-L. 2013, Astron. Astrophys., 551, A138

Ygouf, M., Pueyo, L., Soummer, R., et al. 2015, in Soc. Photo-Opt. Instrum. Eng., Vol. 9605, Techniques and Instrumentation for Detection of Exoplanets VII, 96050S